CLASSIFICATION OF THE SPATIAL EQUILIBRIA OF THE CLAMPED ELASTICA: NUMERICAL CONTINUATION OF THE SOLUTION SET

MICHAEL E. HENDERSON

T. J. Watson Research Center I.B.M.,
Yorktown Heights, NY 10598, USA
mhender@us.ibm.com

SÉBASTIEN NEUKIRCH*

Bernoulli Mathematics Institute, Swiss Federal Institute of Technology,
CH-1015 Lausanne, Switzerland
sebastien.neukirch@epfl.ch

We consider equilibrium configurations of inextensible, unshearable, isotropic, uniform and naturally straight and prismatic rods when subject to end loads and clamped boundary conditions. In a first paper [Neukirch & Henderson, 2002], we discussed symmetry properties of the equilibrium configurations of the center line of the rod. Here, we are interested in the set of all parameter values that yield equilibrium configurations that fulfill clamped boundary conditions. We call this set the *solution manifold* and we compute it using a recently introduced continuation algorithm. We then describe the topology of this manifold and how it comprises different interconnected layers. We show that the border set of the different layers is the well-known solution set of buckled rings.

Keywords: Numerical continuation; boundary value problem for twisted rods; surface following algorithm.

1. Introduction

The equilibrium of a twisted rod is governed by the Kirchhoff (ordinary differential) equations. Here, we study equilibria of twisted rods that are subject to boundary conditions: the rod is held at both ends where moments and forces are applied. The way the rod is held imposes boundary conditions on the solutions of the equilibrium equations. We have to treat a boundary value problem (BVP). A BVP is driven by three numbers: n_{dim} the dimension of the differential system, n_{bc} the number of boundary conditions (that can either be initial conditions or

final conditions), and n_{par} the number of free parameters (parameters of the differential system or parameters that appear in the boundary conditions themselves). The free parameters are sometimes called *global coordinates* of the BVP. They span the n_{par}-dimensional *global representation space*, see [Gáspár *et al.*, 1997]. Of the numbers n_{bc} and n_{dim}, only the difference $k \overset{\text{def}}{=} n_{\text{bc}} - n_{\text{dim}}$ matters: this represents the number of *extra* boundary conditions in the sense that an n_{dim} BVP requires n_{dim} boundary conditions to be well stated (just as an n_{dim} initial value problem requires n_{dim} initial conditions). If the number n_{par} of global coordinates is equal to
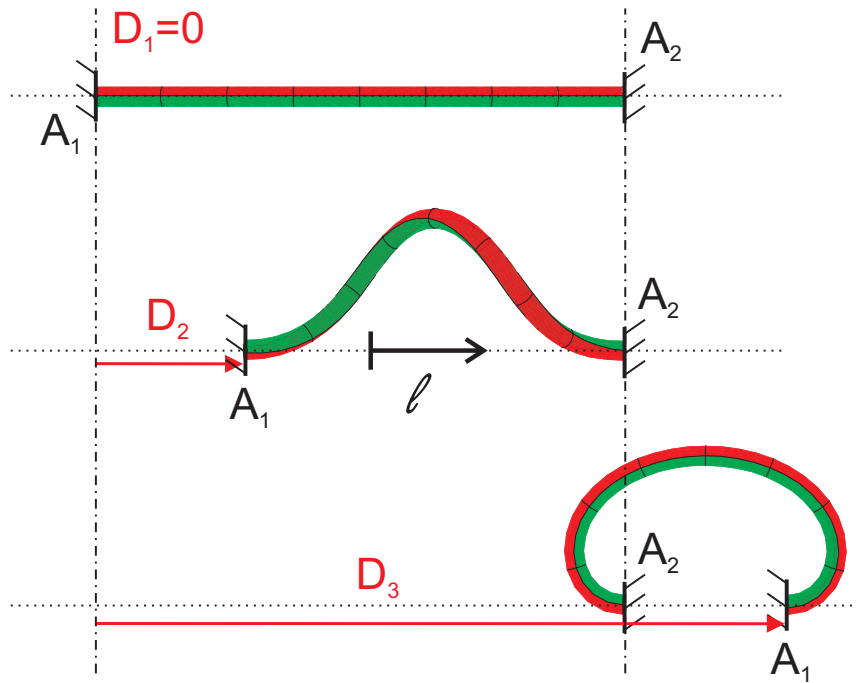
Fig. 1. A rod with clamped boundary conditions: the axis $\boldsymbol{\ell}$ (joining point A_1 to point A_2) and the tangent of the rod at both ends are aligned. The end-shortening D_i of a configuration is the distance between the point A_1 in that configuration and the point A_1 in a straight configuration: $D_1 = 0$, $0 < D_2 < L$ and $L < D_3 < 2L$.

the number k of extra boundary conditions, then the solution set (the set of all global coordinate values that yield solutions of the BVP) consist in one or more disconnected points. Now if $n_{\mathrm{par}} > k$, the solution set will be one (or many) $n_{\mathrm{par}} - k$ dimensional manifold(s) in the n_{par}-D global representation space. Usually only boundary value problems with $n_{\mathrm{par}} - k = 1$ are studied because (1) continuation algorithms are restricted to path following and (2) even when a solution manifold of higher dimension is obtained its complexity hampers its study. Here, we present a case where the global representation space is four-dimensional ($n_{\mathrm{par}} = 4$) and where there are two extra boundary equations ($k = 2$). Hence the solution set is a (or many) surface(s) lying in a 4D space. For a slightly different problem, in [Hoffman *et al.*, 2002] some 2D sheets of the solution set have been computed but via a coordinated family of a one-dimension parameter continuation. We deal with the simplest twisted rod possible: inextensible, unshearable, isotropic, uniform and naturally straight and prismatic. We call it an *ideal elastica*. We choose conservative boundary conditions that correspond to a very natural way of holding and loading an elastic rod: clamped boundary conditions (see Fig. 1). We make use of a

recent algorithm to compute our 2D solution manifold which has two main components: the trivial surface corresponding to straight shapes and the post-buckling surface corresponding to buckled shapes. We show how the post-buckling surface comprises a countable infinity of connected layers and that the scaffolding bearing the layers is the well-known solution set of twisted rings (which are in fact clamped configurations where the two ends join).

The paper is organized as follows: in Sec. 2 we recall the reduction of the equilibrium Kirchhoff equations we introduced in a first paper [Neukirch & Henderson, 2002] and we state the BVP. In Sec. 3 we show how we discretize the BVP and recall the continuation method. In Sec. 4 we describe the properties of the solution manifold.

2. The Model

We study the equilibrium of a rod when subjected to external forces and moments. The rod is taken to be *ideal* i.e. inextensible, unshearable, isotropic, uniform and naturally straight and prismatic. We use the fixed frame $\{\mathbf{e}_x, \mathbf{e}_y, \mathbf{e}_z\}$. As for the director frame $\{\mathbf{d}_1, \mathbf{d}_2, \mathbf{d}_3\}$, we only consider $\mathbf{d}_3$ which is the

tangent to the center line. We have seen [Neukirch & Henderson, 2002] that the equations governing the equilibrium of the center line of such rods can be expressed as two vectorial differential equations.

2.1. *The Kirchhoff statics equations in reduced form*

The way the rod is held (i.e. the boundary conditions) imposes force $\mathbf{f}$ and moment $\mathbf{m}(s)$ on the rod. We have that $\mathbf{f} = $ constant and the moment can be expressed as a function of the center line $\mathbf{r}(s)$:

$$\mathbf{m}(s) = \mathbf{f} \times \mathbf{r}(s) + \mathbf{m}_K, \quad (1)$$

where $\mathbf{m}_K$ is an integration constant which includes $\mathbf{r}(0)$. It shows that $I_0 \stackrel{\text{def}}{=} \mathbf{m}(s) \cdot \mathbf{f}$ is a constant of s. Because we consider boundary conditions involving the center line only, we simply consider the differential equations for it and its tangent:

$$\dot{\mathbf{r}} = \mathbf{d}_3 \quad (2)$$

$$\dot{\mathbf{d}}_3 = (\mathbf{f} \times \mathbf{r} + \mathbf{m}_K) \times \mathbf{d}_3 \quad (3)$$

which have the following integrals of motion:

$$\mathbf{d}_3 \cdot \mathbf{d}_3 = 1, \quad (4)$$

$$I_1 \stackrel{\text{def}}{=} (\mathbf{f} \times \mathbf{r} + \mathbf{m}_K) \cdot \mathbf{d}_3 \ (= m_3) = \text{constant}, \quad (5)$$

$$I_2 \stackrel{\text{def}}{=} \frac{1}{2} |(\mathbf{f} \times \mathbf{r} + \mathbf{m}_K)|^2 + \mathbf{d}_3 \cdot \mathbf{f} = \text{constant}. \quad (6)$$

Note that nondimensionalization has been performed in order that neither the length of the rod (now set to 2π) nor any elastic rigidity appear. Considering Eqs. (2) and (3) as a set of six ordinary differential equations, a rod configuration will depend on both the parameters $(\mathbf{f}, \mathbf{m}_K)$ and the initial conditions $(\mathbf{d}_3(0), \mathbf{r}(0))$. In order to simplify the study, we perform certain choices that do not reduce the generality:

- We choose the origin of the arc-length such that the point $\mathbf{r}(0)$ is at the middle of the rod, i.e. $s \in [-\pi; \pi]$.
- We choose the origin of the fixed frame such that $\mathbf{r}(0) = 0$ (then $\mathbf{m}_K = \mathbf{m}(0)$).
- For the case $\mathbf{f} = 0$ being treated in [Neukirch & Henderson, 2002], we only consider the case of non-null force and choose the $\mathbf{e}_z$ axis along and in the direction of $\mathbf{f} = (0, 0, f > 0)$. The integral of motion I_0 becomes $I_0 = f m_z$, with m_z constant.
- We choose the $\mathbf{e}_x$ and $\mathbf{e}_y$ axes such that the rod at $s = 0$ lies in the $(\mathbf{e}_x, \mathbf{e}_z)$ plane (i.e. $d_{3y}(0) = 0$).

- We note $\mathbf{m}(0) = (m_{x0}, m_{y0}, m_{z0})$. We have seen [Neukirch & Henderson, 2002] that we could restrict our study to solutions with $m_{y0} = 0$ since the ones with $m_{y0} \neq 0$ either do not fulfill clamped boundary conditions or are congruent to solutions having $m_{y0} = 0$. Note that we will refer to m_{z0} as simply m_z since it does not depend on s. The constant m_3 is given by: $m_3 = m_{x0} d_{3x}(0) + m_z d_{3z}(0)$.

2.2. *Symmetries of the solutions*

With $d_{3y}(0) = 0$ and $\mathbf{m}_K = (m_{x0}, 0, m_z)^T$, the solutions of (2) and (3) have the following symmetries:

$$x(-s) = -x(s), \quad y(-s) = y(s),$$
$$z(-s) = -z(s) \quad (7)$$

$$d_{3x}(-s) = d_{3x}(s), \quad d_{3y}(-s) = -d_{3y}(s),$$
$$d_{3z}(-s) = d_{3z}(s) \quad (8)$$

2.3. *Clamped boundary conditions*

We consider the case where the rod is held in a strong anchoring way: on both sides the position and the tangent of the rod are fixed. Moreover in what we call a clamped configuration, the tangent of the rod at both ends is aligned with the axis joining the two ends (see Fig. 1). These clamped boundary conditions can be written as:

$$\mathbf{d}_3(-\pi) = \mathbf{d}_3(\pi) \quad (9)$$

$$\mathbf{r}(\pi) - \mathbf{r}(-\pi) = k \mathbf{d}_3(\pi) \text{ with } k \in] - 2\pi; 2\pi] \quad (10)$$

Using symmetries (7) and (8), the clamped boundary conditions reduce to:

$$d_{3y}(\pi) = 0 \quad (11)$$

$$x(\pi) d_{3z}(\pi) - z(\pi) d_{3x}(\pi) = 0 \quad (12)$$

2.4. *Solution manifold*

Writing, as a definition of the initial value θ_0

$$\mathbf{d}_3(0) = (\sin \theta_0, 0, \cos \theta_0)^T,$$

we see that the system (2), (3) has one free initial condition $\{\theta_0\}$ and three parameters $\{m_z, f, m_{x0}\}$. The problem of finding all the rod configurations which satisfy clamped boundary conditions is equivalent to the problem of finding all the set of values of the global coordinates $\{m_z, f, m_{x0}, \theta_0\}$ for which the integration of (2), (3) yields solutions that fulfill

Eqs. (11) and (12). Hence in the 4D global representation space spanned by $\{m_z, f, m_{x0}, \theta_0\}$, we are looking for the 2D solution manifold implicitly defined by Eqs. (11) and (12). The computation of this solution manifold is explained in Sec. 3. It has the following discrete symmetries:

$$(m_z, f, m_{x0}, \theta_0) \rightarrow (-m_z, f, -m_{x0}, \theta_0)$$
$$\text{with} \quad (x, d_{3x}, y, d_{3y}, z, d_{3z}) \rightarrow (x, d_{3x}, -y, -d_{3y}, z, d_{3z}) \tag{13}$$

$$(m_z, f, m_{x0}, \theta_0) \rightarrow (m_z, f, -m_{x0}, -\theta_0)$$
$$\text{with} \quad (x, d_{3x}, y, d_{3y}, z, d_{3z}) \rightarrow (-x, -d_{3x}, -y, -d_{3y}, z, d_{3z}) \tag{14}$$

$$(m_z, f, m_{x0}, \theta_0) \rightarrow (m_z, -f, m_{x0}, \theta_0 + \pi)$$
$$\text{with} \quad (x, d_{3x}, y, d_{3y}, z, d_{3z}) \rightarrow (-x, -d_{3x}, -y, -d_{3y}, -z, -d_{3z}) \tag{15}$$

Symmetry 13 is what is left of the continuous register symmetry. Symmetry 14 comes from the freedom of choosing the orientation of the $\mathbf{e}_x$ axis. Symmetry 15 comes from the freedom of choosing the orientation of the $\mathbf{e}_z$ axis, hence the sign of the constant f which is here taken positive.

2.5. *End shortening*

We define the end-shortening d as:

$$d \overset{\text{def}}{=} 1 - \frac{(\mathbf{r}(\pi) - \mathbf{r}(-\pi)) \cdot \mathbf{d}_3(\pi)}{2\pi} = 1 - \frac{k}{2\pi}. \tag{16}$$

This is the difference of the distance between the ends when the rod is buckled compared to the distance between the ends when the rod is straight ($= 2\pi$). Circularly closed configurations (also called rings) have $d = 1$. Taking into account the symmetries of the center line we can write:

$$d = 1 - \frac{x(\pi)d_{3x}(\pi) + z(\pi)d_{3z}(\pi)}{\pi}. \tag{17}$$

It is sometimes assumed that the rod has constant values of the end shortening. The problem then boils down to following 1D-curves on the 2D solution manifold (see [Coleman & Swigon, 2000; Li & Maddocks, 1994; Dichmann *et al.*, 1996]). This can be done by using classic path following algorithms, see [Allgower & Georg, 1997; Govaerts, 2000; Beyn *et al.*, 2002] and references therein.

3. Numerics: Discretization and Continuation

The reduced 6D system is:

$$\dot{x} = d_{3y} \quad \dot{d}_{3x} = fxd_{3z} - m_z d_{3y}$$
$$\dot{y} = d_{3y} \quad \dot{d}_{3y} = fyd_{3z} - m_{x0}d_{3z} + m_z d_{3x}$$
$$\dot{z} = d_{3z} \quad \dot{d}_{3z} = -fxd_{3x} - fyd_{3y} + m_{x0}d_{3y}.$$

$$x(0) = 0 \quad d_{3x}(0) = \sin\theta_0$$
$$y(0) = 0 \quad d_{3y}(0) = 0 \tag{18}$$
$$z(0) = 0 \quad d_{3z}(0) = \cos\theta_0$$

$$d_{3y}(\pi) = 0$$
$$x(\pi)d_{3z}(\pi) - z(\pi)d_{3x}(\pi) = 0$$

We wish to compute the solution manifold of this system over some part of the global representation space. We first discretize using a conservative second-order finite difference scheme, then use a recently developed continuation method to find a polygonal tiling of the surface.

3.1. *Discretization of the reduced 6D system*

We discretize Eq. (18) using the Keller box scheme [Keller, 1976] which is second-order, and stable. With a nonuniform mesh $\{s_i\}$, for $i = 0, \ldots, N$, and

$$\frac{s_0 + s_1}{2} = 0, \quad s_{i-1} < s_i, \quad \frac{s_{N-1} + s_N}{2} = \pi$$

and the notation (with $h_i = s_{i+1} - s_i$)

$$Ag(s_{i+\frac{1}{2}}) \overset{\text{def}}{=} \frac{g(s_{i+1}) + g(s_i)}{2}$$
$$= g\left(\frac{s_{i+1} + s_i}{2}\right) + O(h_i^2) \tag{19}$$

$$Dg(s_{i+\frac{1}{2}}) \overset{\text{def}}{=} \frac{g(s_{i+1}) - g(s_i)}{s_{i+1} - s_i}$$
$$= \dot{g}\left(\frac{s_{i+1} + s_i}{2}\right) + O(h_i^2) \tag{20}$$

the box scheme is then

$$Dx = Ad_{3x} \qquad\qquad Dd_{3x} = f A x A d_{3z} - m_z A d_{3y}$$

$$Dy = Ad_{3y} \qquad\qquad Dd_{3y} = f A y A d_{3z} - m_{x0} A d_{3z} + m_z A d_{3x}$$

$$Dz = Ad_{3z} \qquad\qquad Dd_{3z} = -f A x A d_{3x} - f A y A d_{3y} + m_{x0} A d_{3y}$$

$$Ax(s_{\frac{1}{2}}) = 0 \qquad\qquad Ad_{3x}(s_{\frac{1}{2}}) = \sin\theta_0$$

$$Ay(s_{\frac{1}{2}}) = 0 \qquad\qquad Ad_{3y}(s_{\frac{1}{2}}) = 0$$

$$Az(s_{\frac{1}{2}}) = 0 \qquad\qquad Ad_{3z}(s_{\frac{1}{2}}) = \cos\theta_0 \,.$$

$$Ax(s_{N-\frac{1}{2}})Ad_{3z}(s_{N-\frac{1}{2}}) - Az(s_{N-\frac{1}{2}})Ad_{3x}(s_{N-\frac{1}{2}}) = 0$$

$$Ad_{3y}(s_{N-\frac{1}{2}}) = 0$$

This is a second-order approximation for both the differential equation and the boundary conditions, and it has the same invariants as the differential equation. Note that for any two functions $u(s)$ and $v(s)$:

$$D(u(s_{i+\frac{1}{2}})v(s_{i+\frac{1}{2}})) \equiv Au(s_{i+\frac{1}{2}})Dv(s_{i+\frac{1}{2}})$$
$$+ Du(s_{i+\frac{1}{2}})Av(s_{i+\frac{1}{2}}) \quad (21)$$

Using the discrete equations, and this identity, we have

$$D(d_{3x}^2 + d_{3y}^2 + d_{3z}^2) = D(\mathbf{d}_3 . \mathbf{d}_3) = 0$$

$$D(fx^2 + fy^2 - 2m_{x0}y + 2d_{3z}) = DI_1 = 0 \,.$$

$$D(fxd_{3y} + (m_{x0} - fy)d_{3x} + m_z d_{3z}) = DI_2 = 0 \,.$$

So if exact floating computations were done, the difference scheme would preserve the same quantities as the differential equations.

3.2. *Continuation*

The discrete equations are a nonlinear system of the form

$$F(u), \quad F : \mathbb{R}^{6N+10} \to \mathbb{R}^{6N+8} \,.$$

The dimension $6N + 10$ comes from the fact that at each of the $N + 1$ mesh points we have six quantities $(x, y, z, d_{3x}, d_{3y}, d_{3z})$, and that we have four free parameters $(m_z, f, m_{x0}, \theta_0)$. The dimension $6N + 8$ comes from the fact that we write matching equations at N points for the six quantities $(x, y, z, d_{3x}, d_{3y}, d_{3z})$ and besides that we have eight boundary conditions. We use the multiple parameter continuation algorithm, described in detail in [Henderson, 2002], to compute the solutions of this system. This algorithm requires two calculations: finding a basis for the null space of the Jacobian F_u (this is the tangent space of the solution
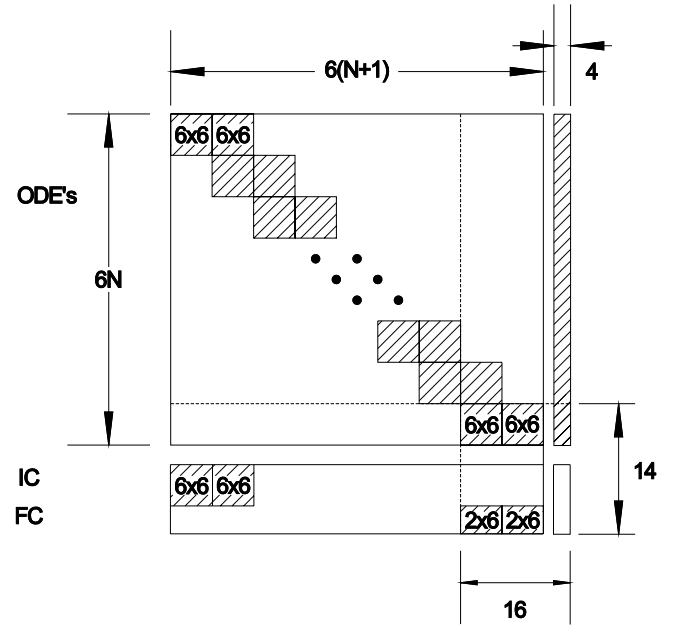

Fig. 2. The block structure of the Jacobian F_u. IC stands for initial conditions. FC stands for final conditions.

manifold), and projecting a point onto the manifold orthogonal to the tangent space.

The Jacobian F_u is a bordered band matrix with a border of four columns corresponding to derivatives w.r.t $(m_z, f, m_{x0}, \theta_0)$, and eight rows corresponding to the boundary conditions. It is a rectangular system. We can find a basis for the tangent space Φ (a $(6N+10) \times 2$ matrix with orthonormal columns), by finding a basis for the null space of the Jacobian

$$F_u(u)\Phi = 0 \,.$$

This is done by the usual version of Gaussian elimination for banded systems with partial pivoting for the first $6(N-1)$ equations, which leaves a 14×16 submatrix. Then, by appending two zero rows, the Lapack singular value decomposition can be used

on that subblock to find a basis for the null space. The basis in the original coordinates can then found by back-solves.

Projecting a point $\mathbf{s}$ in the tangent space at a point u_i onto $F = 0$ orthogonal to the tangent space means solving the nonlinear system for u:

$$F(u) = 0\,,$$

$$\Phi^T(u - u_i) = \mathbf{s}$$

We use Newton's method and the same modified band solver. The Jacobian has the same block structure as above, but two full rows have been added, which makes it a $(6N + 10) \times (6N + 10)$ system. Partial pivoting to eliminate the first $6(N-1)$ equations results in a full 16×16 submatrix which we factor using full pivoting. If the Jacobian $F_u(u_i)$ is full rank the Jacobian of this bordered system is nonsingular, so there will be some ball $|s| < R$ in which Newton's method converges starting from $\tilde{u} = u + \Phi s$.

With these two operations, we can find a polygonal tiling of $F(u) = 0$. This will be done using polygons in the tangent spaces Φ_i, at a set of points $\{u_i\}$

$$F(u_i) = 0\,, \quad i = 0, \ldots, m - 1\,.$$

Each point has an associated polygon P_i, which is initially a square, and which is updated by subtracting a half-plane at each step of the continuation. We begin with an initial point u_0 and one tile M^0 (tile i is the set of points $u_i + \Phi_i s$, where $|s| \leq R_i$ and s lies in the polygon P_i)

$$F(u_0) = 0\,,$$

$$M^0 = \{u_0, R_0, \Phi_0, P_0\}$$

$$P_0 = |\mathbf{s}|_\infty \leq R_0\,.$$

At each step of the algorithm we select a new point u_m, which is the projection of a point $\mathbf{s}_m$ on tile i onto $F = 0$. Tile i is chosen such that the polygon P_i has at least one vertex which is outside the circle $|\mathbf{s}| = R_i$. If $v \in \text{vertices}(P)$ and $|v_m| > R_i$, $s_m = R_i v_P / |v_P|$. If the polygons are updated according to the procedure described below, this guarantees that the new point u_m is not closer than R_j to any other point u_j (see [Henderson, 2002]). This keeps the continuation moving outward.

The polygon for tile m is initially the square $P_m = \{s \| \mathbf{s}\|_\infty \leq R_m\}$. We identify each tile i that overlaps the new tile, $(|u_m - u < i| \leq R_m + R_i)$, and
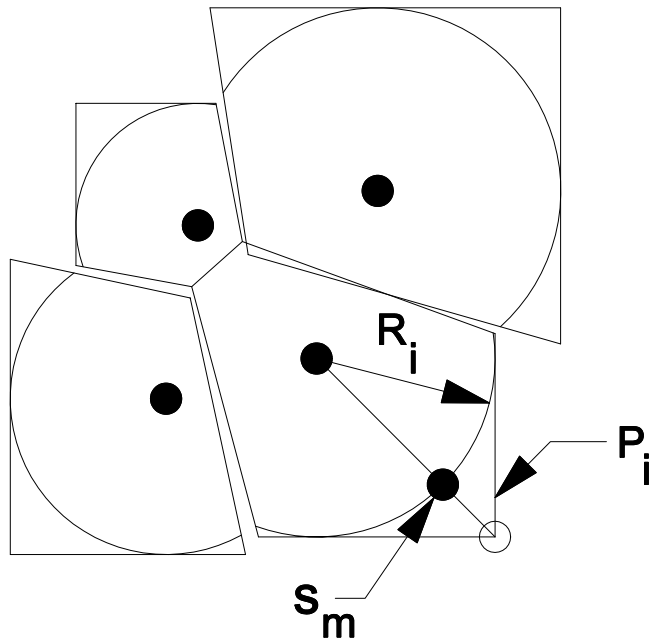

Fig. 3.   The basis of the continuation: a new tile is added for any u_i whose polygon P_i has a vertex outside $|\mathbf{s}| = R_i$. The new tile is centered at a point which is the projection onto $F = 0$ of the intersection of a line between the origin and the exterior vertex and the circle $|\mathbf{s}| = R_i$. The figure represents the projection of nearby tiles into the tangent space at u_i.
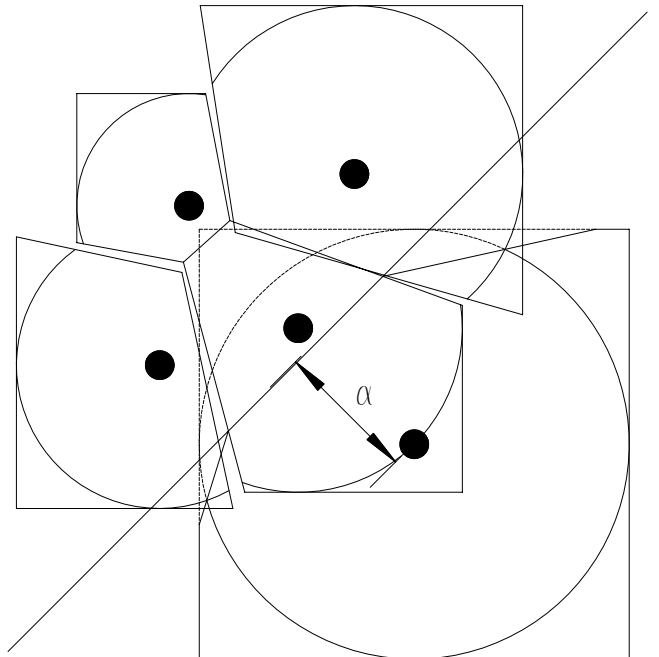

Fig. 4.   Updating the polygons: one half-plane is removed for each overlapping point. Again, the figure represents the projection of nearby points and polygons into the tangent space at u_i. If the manifold were flat the half spaces defined by α_{im} and α_{mi} are complementary, so there would be no gap between the polygons.

subtract a half-plane from polygons P_m and P_i:

$$P_i \leftarrow P_i \cap \{s | s \cdot \Phi_i^T (u_i - u_m) \le \alpha_{im}\}$$

$$P_m \leftarrow P_m \cap \{s | s \cdot \Phi_m^T (u_m - u_i) \le \alpha_{mi}\}$$

$$\alpha_{ij} = \frac{1}{2} \left(1 + \frac{R_i^2 - R_j^2}{|u_j - u_i|^2} \right).$$

In the figures showing the surface we draw the polygons in the tangent space, so that the surface is made up of planar polygonal facets. The gaps are due to the projections into different tangent spaces, and the size of the gaps (and the distance between a point in the polygon and its projection onto the surface) is related to the ratio of the radius and the curvature of the surface. We have chosen the radius so that this is less than a prescribed tolerance.

4. Results and Discussion

We applied this algorithm to the nonlinear two-point boundary value problem defined by (2), (3), (11) and (12). The computation was done in the domain $-10 \le m_z \le 10$, $-10 \le m_{x0} \le 10$, and $0 \le f \le 16$, with 100 mesh points. An initial point on the manifold was obtained by shooting, and the continuation was restricted to the first octant ($mz \ge 0$, $m_{x0} \ge 0$, $f \ge 0$) and θ_0 was considered modulo 2π. At points where the manifold crosses the symmetry planes $m_z = 0$ or $m_{x0} = 0$, symmetries (13) or (14) were used to get new seed points (and hence new parts of the manifold) without leaving the first octant. Provided the domain is chosen large enough, we could get the complete first eight layers ($n = 1^-$ to $n = 4^+$) and some parts of higher n layers.

4.1. *Special curves*

The solution manifold comprises different important paths in the parameter space $(m_z, m_{x0}, \theta_0, f)$.

4.1.1. *Buckling curves*

The trivial planes $\{\theta_0 = 0 \bmod \pi, m_{x0} = 0\}$ correspond to configurations of straight rod ($d = 0$) twisted or not. On these planes, buckling curves connect straight solutions to buckled solutions ($d > 0$). When $\theta_0 = 0 \bmod 2\pi$ the equation of the buckling curves is:

$$(\cos \pi \sqrt{m_z^2 - 4f} - \cos \pi m_z) \sqrt{m_z^2 - 4f}$$

$$= 2\pi f \sin \pi \sqrt{m_z^2 - 4f}, \text{ with } m_z^2 > 4f. \quad (22)$$
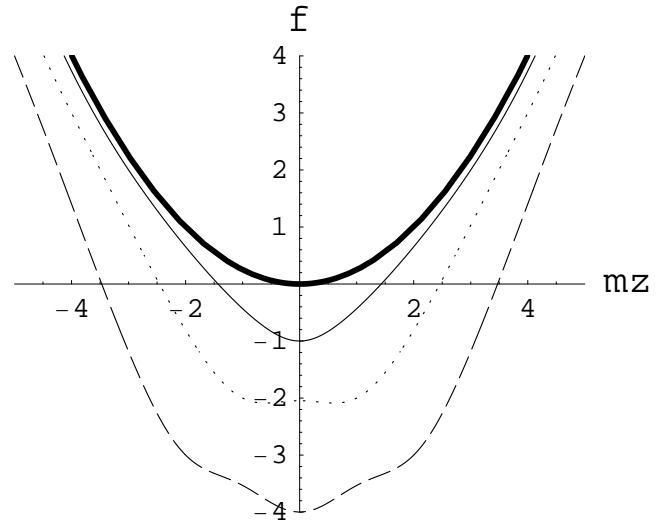

Fig. 5.   The thick line ($m_z^2 = 4f$) is the buckling curve for a rod of infinite length; while the plain, dotted, dashed curves are the curves of the first, second and third (resp.) buckling modes for a finite rod [Eq. (22)].

Equation (22) defines a countable infinity of curves. Each curve corresponds to a buckling mode. The buckling mode are numbered $b = 1, 2, 3$ starting with the curve nearest to the origin (see Fig. 5). Since we restrict our study to positive f, we use the symmetry (15) to fold the ($f < 0$, $\theta_0 = 0$) part of each buckling curve to ($f > 0$, $\theta_0 = \pi$). Note that at $f = 0$, the freedom of choosing the z axis implies a degeneracy for the angle θ_0 which results in the presence of two buckling circles: $(f, m_z, m_{x0}) = \pm w_b (0, \cos \theta_0, \sin \theta_0)$, where w_b is the bth strictly positive solution of $\tan \pi w_b = \pi w_b$.

4.1.2. *Planar (untwisted) elastica curves*

Other important paths are curves corresponding to the planar elastica solutions (defined by $\{m_3 = 0, I_1 = 0\}$). Planar elastica are divided into two families: inflexional and noninflexional [Love, 1944].

The curves for the pth noninflexional planar elastica are:

$$\pi m_{x0} = 2pK\left(\frac{4f}{m_{x0}^2}\right) \quad \text{and } \theta_0 = \pi \bmod 2\pi \quad (23)$$

$$\pi m_{x0} = 2pK\left(-\frac{4f}{m_{x0}^2}\right) \quad \text{and } \theta_0 = 0 \bmod 2\pi \quad (24)$$

where $K(m)$ is the complete elliptic integral of the first kind (see Appendix of [Neukirch & Hender-

son, 2002]). Again we only consider the $f \geq 0$ part of these curves. Then on (23) $d \leq 1$ (resp. $d \geq 1$) when p is odd (resp. even). And on (24) $d \geq 1$ (resp. $d \leq 1$) when p is odd (resp. even).

The curve for the pth (p odd) inflexional planar elastica is:

$$\pi\sqrt{f} = (p+1)K\left(\frac{m_{x0}^2}{4f}\right)$$

$$\text{and} \quad \theta_0 = \pi \bmod 2\pi \quad (0 \leq d < 2) \quad (25)$$

The curve for the pth (p even) inflexional planar elastica is:

$$-2\sqrt{\frac{m}{2}} \cos \hat{s}_\pi \cos \theta_\pi$$

$$= (-1)^{\frac{p}{2}} \operatorname{sign}(\sin \theta_0)\sqrt{1 - \cos^2 \theta_\pi}$$

$$\times \left(\pi - \frac{2}{\sqrt{f}}\left(E(\hat{s}_\pi, m) - E(m)\right)\right)$$

$$\text{and} \quad m_{x0} = 0 \quad (0 \leq d < 2) \quad (26)$$

with $m = (\cos\theta_0 + 1)/2$, $\hat{s}_\pi = \operatorname{am}(\pi\sqrt{f} + K(m), m)$ and $\cos\theta_\pi = -1 + (\cos\theta_0 + 1)\sin^2(\hat{s}_\pi)$.

4.1.3. *Planar rings (twisted or not)*

Planar rings correspond to helices ($u_- = u_0$) of null pitch angle ($\theta(s) \equiv \theta_0 = (\pi/2) + k\pi$). They lie on the subset $m_3 m_z = f$ of the post-buckling surface. This corresponds to:

+ N-covered planar untwisted rings at: $f = 0$, $m_z = -N\sin\eta$, $m_{x0} = N\cos\eta$, with $\eta = \theta_0 \bmod \pi$.
+ N-covered planar twisted rings at: $m_z = \pm N$, $\theta_0 = (\pi/2) + k\pi$, $f = (-1)^k m_z m_{x0}$ (k integer).

4.2. *Surface when length is infinite*

Now the global post-buckling surface has somehow to include all these special paths. Let us start by considering what happens in the case of infinite length (with $f \geq 0$). The configuration of the rod is associated with the homoclinic orbit in the phase plane (θ, ω) when $m_3 = m_z$ and $f > (1/4)m_z^2$ (see [Neukirch & Henderson, 2002; van der Heijden & Thompson, 2000]). There is only one buckling curve:

$$m_z^2 = 4f, \quad m_{x0} = 0 \quad \text{and} \quad \theta_0 = 0 \bmod 2\pi \quad (27)$$

and there is only one path for the planar elastica:

$$m_{x0}^2 = 4f, \quad m_z = 0 \quad \text{and} \quad \theta_0 = \pi \bmod 2\pi \quad (28)$$
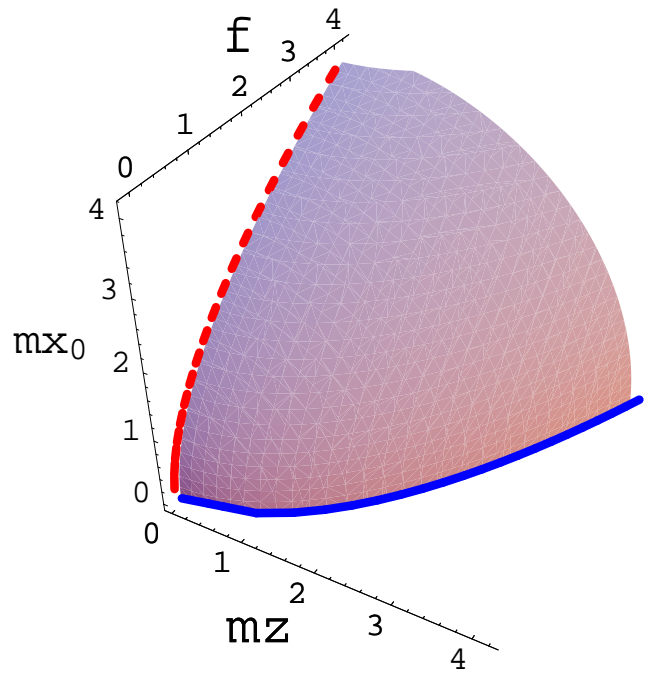

Fig. 6. Post-buckling surface in the case of infinite length (homoclinic orbit). The surface joins the buckling curve (plain blue, $\theta_0 = 0$) to the planar curve (dotted red, $\theta_0 = \pi$).

and the post-buckling surface:

$$m_{x0}^2 + m_z^2 = 4f \quad \text{with} \quad \theta_0 = 2\arctan\left(\frac{m_{x0}}{m_z}\right) \in [0; \pi] \quad (29)$$

simply joins the buckling curve to the planar elastica curve (see Fig. 6).

As we go from infinite length to finite length, we see that the unique buckling curve splits up into different buckling modes. In the same way the unique planar elastica path splits up into different paths. We may then imprudently conclude that in the finite length case, the solution manifold consists of disconnected layers, each layer connecting the bth buckling curve to the pth planar curve with $b = p$. The first problem is that each p planar elastica path is in fact made of two paths: inflexional and non-inflexional, so there cannot be a one-to-one correspondence with the $b = p$ buckling mode.

It turns out that the post-buckling surface is not disconnected, but nevertheless can be divided in layers. Each layer contains solutions for which the period T in the phase plane (θ, ω) is such that the pulsation:

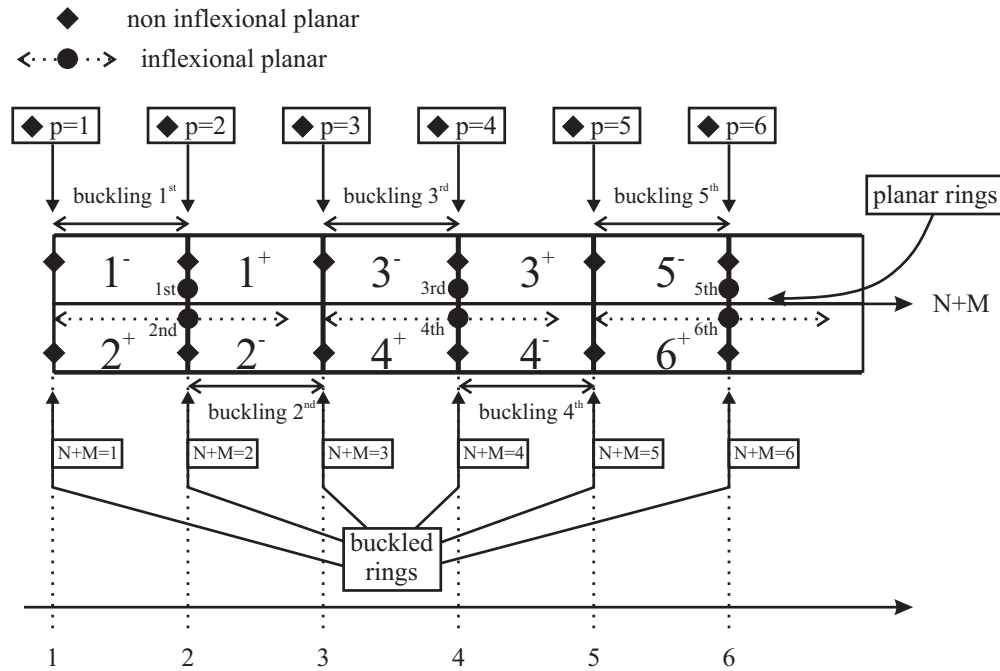$$\Omega = \frac{2\pi}{T} \quad (30)$$

Fig. 7. Sketch of the disposition of the different layers of the post-buckling surface together with important special paths of solutions (corresponding to planar or closed configurations). The harmonics are sorted according to their $\Omega = N + M$ value. The borders that part the different harmonics are the buckled rings that appear for integer value of Ω and the twisted planar rings that exist for continuous value of Ω. All planar configurations but even inflexional ones have an integer Ω. Above (resp. under) the line of planar twisted rings, $u_- > u_0$ (resp. $u_- < u_0$) and $u_- = u_0$ on the line.

is bounded by two following integers (see Fig. 7). The period T is the period of $\theta(s)$ and can be tracked numerically with $d_{3z}(s) = \cos \theta(s)$. The layers are labeled with an integer n:

$$(\text{odd}) \quad n = 1 + 2 \, \text{Int}\left(\frac{\Omega - 1}{2}\right) \quad \text{if } u_- > u_0, \quad (31)$$

$$(\text{even}) \quad n = 2 + 2 \, \text{Int}\left(\frac{\Omega - 1}{2}\right) \quad \text{if } u_- < u_0, \quad (32)$$

where $u_- = \cos \theta(s = T/2)$, $u_0 = \cos \theta_0$ and $\text{Int}(x) = i$ such that $i \leq x < i + 1$. The label n is completed by a sign $\pm$ which is the sign of $d - 1$ with d given by Eq. (16). Nevertheless, numerics show that all the different layers asymptotically ($f \to +\infty$) tend either to (29) or to the set ($m_{x0} = 0$, $\theta_0 = 0$, $m_z^2 \leq 4f$). This accumulation of layers at large f explains numerical difficulties encountered there (see [Domokos & Holmes, 1993; Karolyi & Domokos, 1999]).

4.3. *Connectivity of the layers*

Here are the properties of the layers:

- Each n^- layer contains the $d \in [0, 1]$ part of the nth inflexional planar elastica. And each n^+ layer

contains the $d \in [1, 2]$ part of the nth inflexional planar elastica. This property can be used to actually compute each layer by a 2D continuation: to get the $n^\pm$ layer we take starting point(s) along the corresponding inflexional planar elastica and we do not permit the continuation to cross the $d = 1$ set.

- Each layer n^- contains the nth buckling curve, but also the $d \in [0, 1]$ part of the path of the nth noninflexional planar elastica [Eq. (23) (resp. (24)) with $p = n$ for n odd (resp. n even)].
- Each layer n^+ contains the $d \in [1, 2]$ part of the path of the pth noninflexional planar elastica [Eq. (23) (resp. (24)) with $p = n + 1$ (resp. $p = n - 1$) for n odd (resp. n even)].
- Each layer $n^\pm$ has a part going to $f \to +\infty$ (each part n^- is connected to the buckling curve which goes to $f \to +\infty$ and each part n^+ is connected to the nth inflexional planar elastica path which goes to $f \to +\infty$).

A natural question arises: what happens when we change layer? Or put another way: what are the boundaries of the layers? We have seen [Neukirch & Henderson, 2002] that if starting with a (clamped) configuration with label $n^\pm$

and wanting to continually deform it to another (clamped) configuration with a different label, we had to pass through a circularly closed configuration (i.e. $d = 1$). Hence in the parameter space the different layers $n^\pm$ are bounded by the set of solutions with $d = 1$: planar or buckled rings.

4.4. *The $d = 1$ skeleton*

The set of closed configurations plays the role of the skeleton of the post-buckling surface: it connects the $n^\pm$ layers with one another. Closed solutions are of two kinds: planar rings and buckled (3D) rings. These configurations have been extensively studied in [Li & Maddocks, 1994; Dichmann *et al.*, 1996]. There, a strictly positive integer N was defined to account for the covering of the ring: the number of times the center line of the rod covers itself. Along the planar ring branches $N = |m_z|$ and the twisting moment $m_3 = \pm m_{x0}$. As stated in [Li & Maddocks, 1994], on a branch of N-covered planar rings, branches of buckled rings are going to bifurcate each time

$$|m_{x0}(N, M)| = \sqrt{M + 2N}\sqrt{M}, \qquad (33)$$

with M a strictly positive integer labeling the buckling modes. The two integers (N, M) were used to label the buckled ring branches. It has been remarked that the (N_1, M_1) branch emanating from the M_1th bifurcation point of the N_1-covered planar ring branch eventually joining the N_1th bifurcation point of the M_1-covered planar ring branch. In short N and M could be exchanged.

This property is consistent with our present findings: we first redefine the label M along a planar twisted ring branch:

$$M \overset{\text{def}}{=} \sqrt{N^2 + m_{x0}^2} - N. \qquad (34)$$

Hence M monotonically increases with the twisting moment, $M \in [0; +\infty[$, and bifurcation points correspond to M reaching integer values. Moreover along planar ring branches, as seen in [Neukirch & Henderson, 2002], $\Omega = \sqrt{m_z^2 + m_{x0}^2}$ which yields

$$\Omega = M + N. \qquad (35)$$

At a bifurcation point Ω is then an integer and along the buckled ring branch emanating from this bifurcation point, Ω is to keep this integer value: otherwise the trajectory in phase plane would cease to be closed and the rod shape would cease to be a ring (see [Neukirch & Henderson, 2002]). This property of constant Ω along the buckled ring branches can

be seen as a necessary (but not sufficient) condition of the exchanging $N \leftrightarrow M$ property mentioned above.

We should add that as seen in [Neukirch & Henderson, 2002], in the case of closed rods, the translational invariance in arc-length $(s \rightarrow s + \delta)$ implies that solutions with $m_{y0} \neq 0$ exist. Associated to any closed solution with $(m_z, m_{x0}, \theta_0, f)$ and $m_{y0} = 0$, there are solutions of same shape with the same m_z and f but with $\tilde{m}_{y0} \neq 0$, $\tilde{\theta}_0$ and $\tilde{m}_{x0}$ such that:

$$m_{x0} \sin \theta_0 + m_z \cos \theta_0$$
$$= m_3 = \tilde{m}_{x0} \sin \tilde{\theta}_0 + m_z \cos \tilde{\theta}_0 \qquad (36)$$

and

$$\frac{1}{2}(m_{x0}^2 + m_z^2) + f \cos \theta_0$$
$$= I_2 = \frac{1}{2}(\tilde{m}_{x0}^2 + \tilde{m}_{y0}^2 + m_z^2) + f \cos \tilde{\theta}_0. \qquad (37)$$

This defines a set of 1D continuum, each equivalent to S^1, of solutions associated with each discrete solution we compute. This together with the continuum associated with the registered symmetry yield the T^2 torus of solutions studied in [Li & Maddocks, 1994; Dichmann *et al.*, 1996; Domokos & Healey, 2001].

4.5. *Description of the figures*

The continuation code can output the data in different formats (e.g. the VBM file format [Paffenroth, 1998]). We have used OpenDX to post-process the data and plot the figures presented here. We show θ_0 projections of the layers in the half space $(m_z, m_{x0}, f \geq 0)$. Due to symmetry (15) the projections in the $f \leq 0$ are the same. We also make use of the two other symmetries (13) and (14) to only show a quarter of each layer $n\pm$. Nevertheless each one of these quarters does not correspond to the truncation of the layers in a specified octant of the $(m_z, m_{x0}, f \geq 0)$ half space. Indeed the quarters we show do cross the planes $m_z = 0$ or $m_{x0} = 0$.

In Sec. 4.3 we stated that each $n\pm$ layer comprises an inflectional elastica path and a noninflexional elastica path. We now use these paths (instead of the $m_z = 0$ or $m_{x0} = 0$ planes) to clip each layer into four quarters. A *quarter* is defined as a part of a layer that joins the inflectional and noninflectional planar elastica paths. A layer, which is itself bounded by $d = 1$ paths, contains four quarters
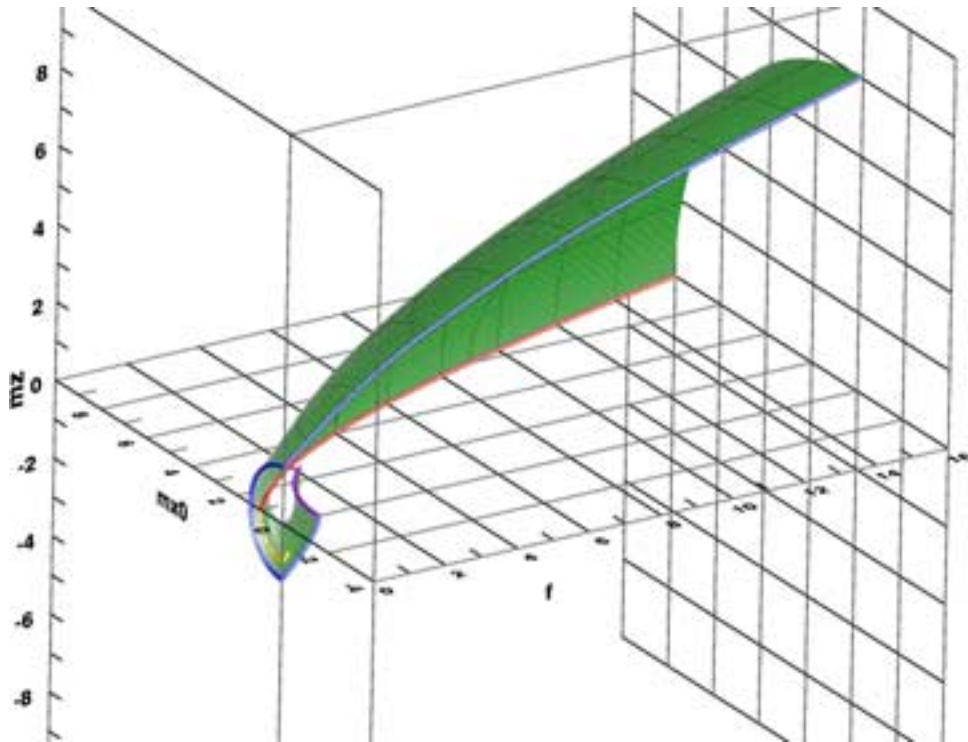
Fig. 8. A quarter of layer 1− in the half space $(m_z, m_{x0}, f \geq 0)$. Yellow curves correspond to twisted rings (either planar or buckled), orange circles (at $f = 0$) to untwisted planar rings, red curves to noninflexional planar elastica, and purple curves to inflexional planar elastica. Blue curves are the buckling curves.
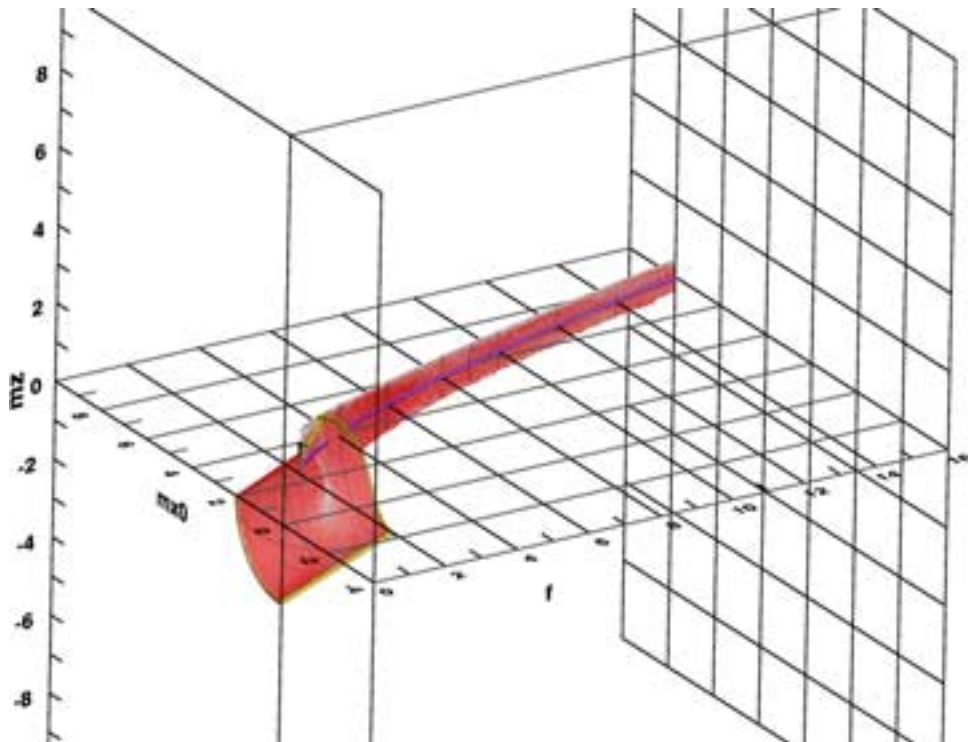

Fig. 9. A quarter of layer 1+ in the half space $(m_z, m_{x0}, f \geq 0)$.
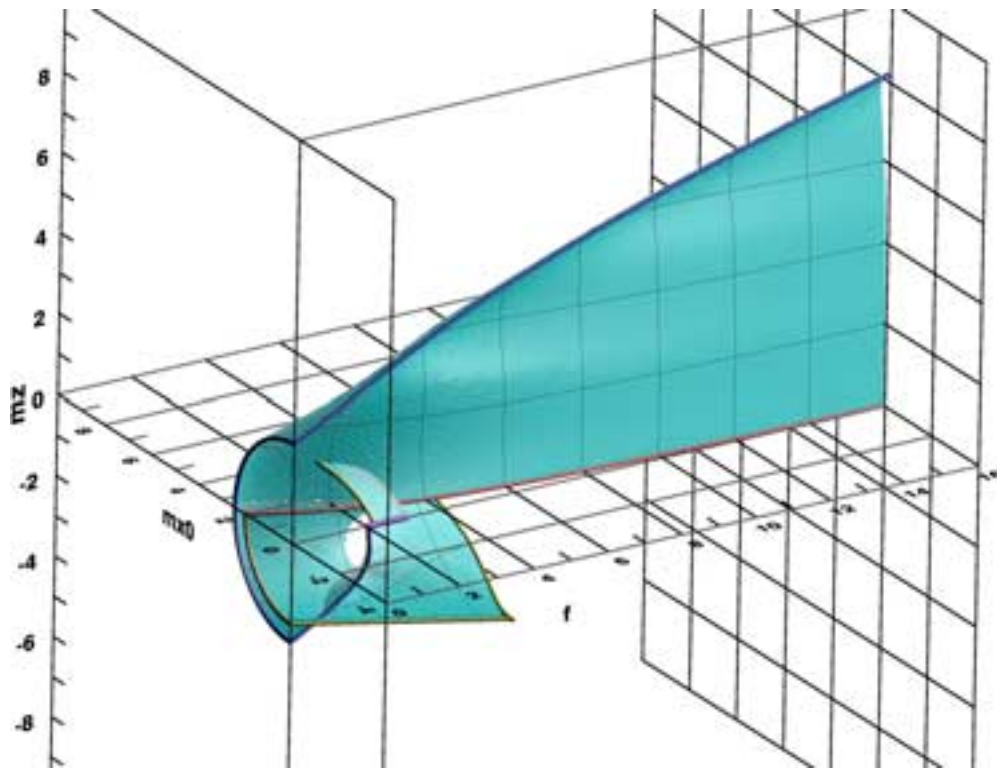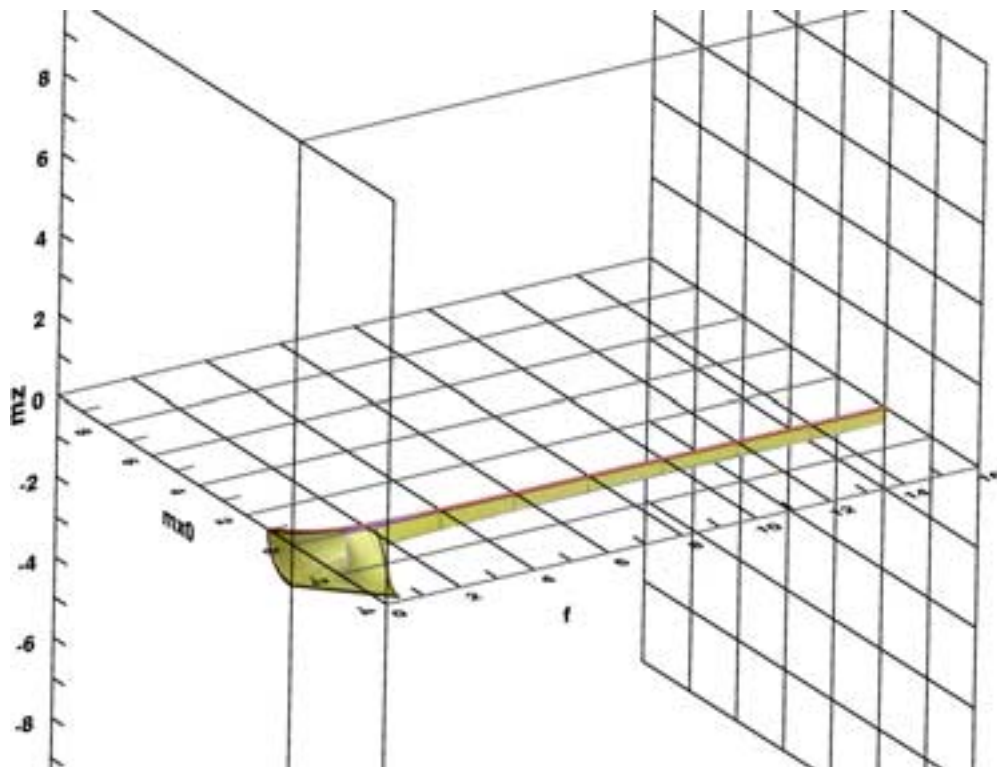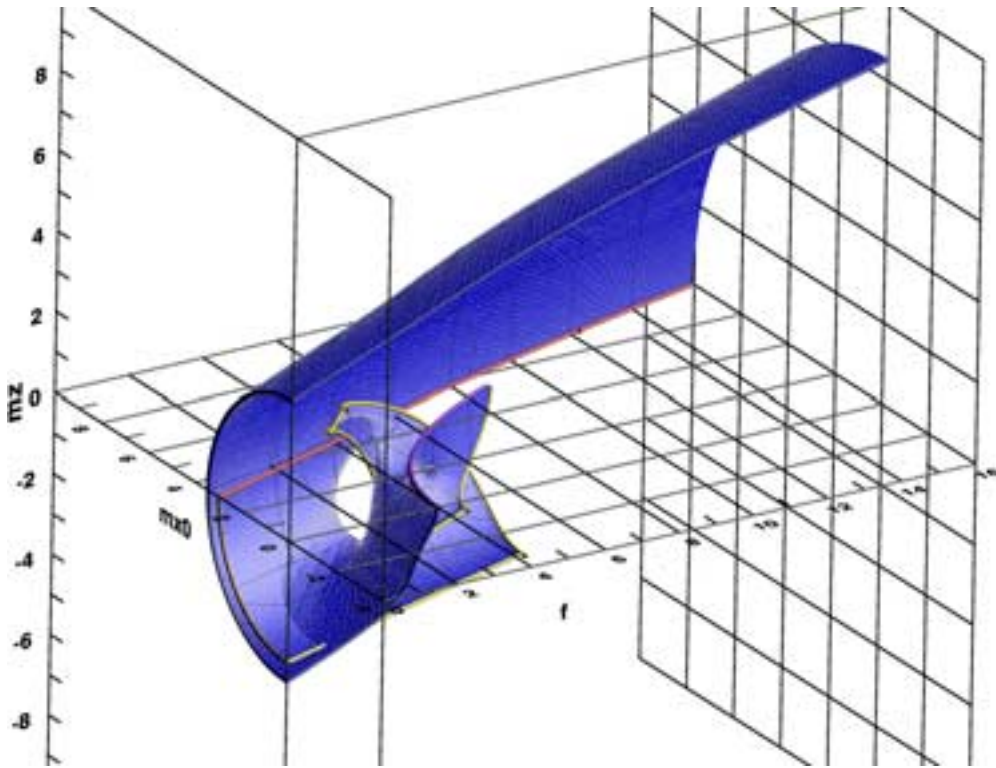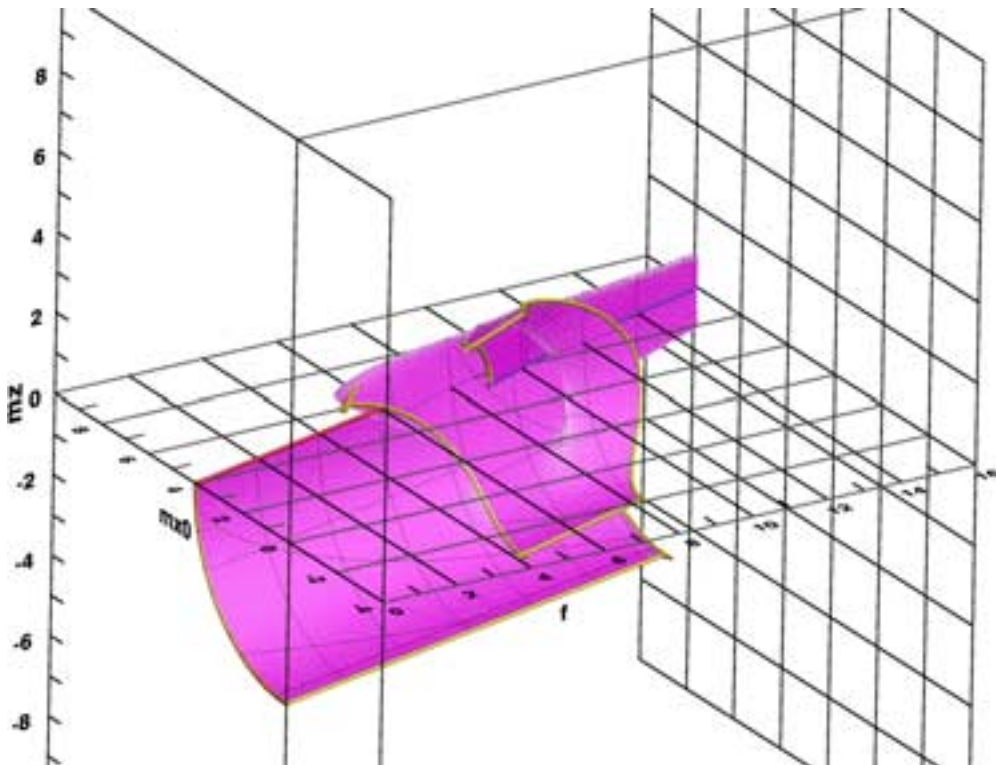
Fig. 10.   A quarter of layer 2− in the half space $(m_z, m_{x0}, f \geq 0)$.

Fig. 11.   A quarter of layer 2+ in the half space $(m_z, m_{x0}, f \geq 0)$.

Fig. 12. A quarter of layer 3− in the half space $(m_z, m_{x0}, f \geq 0)$.

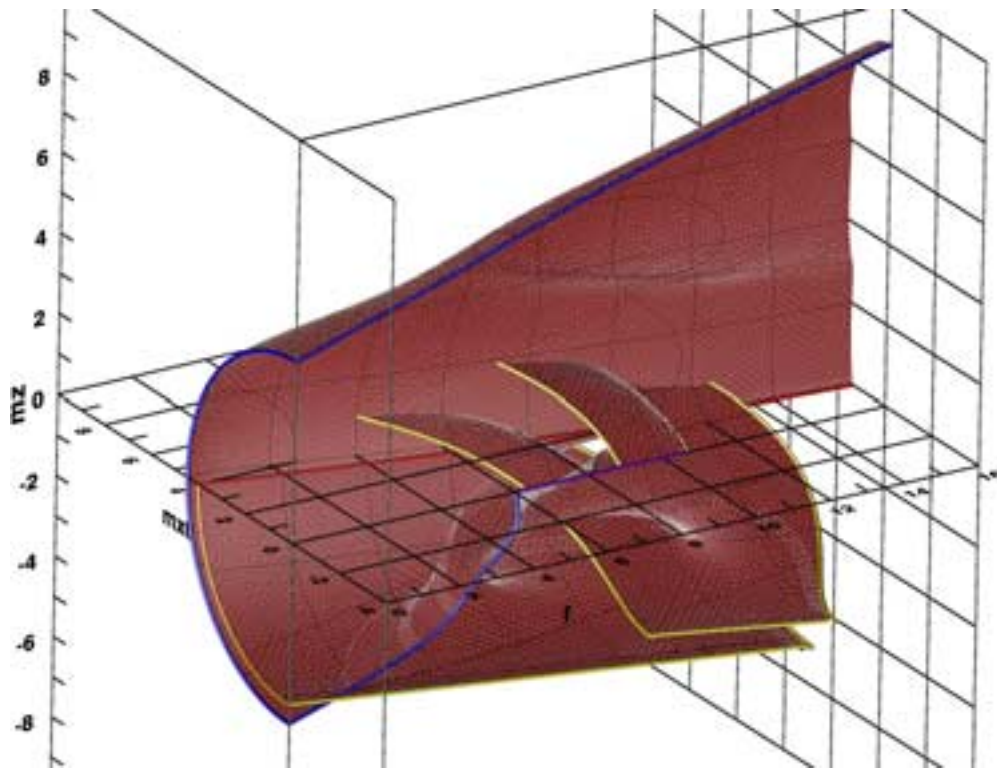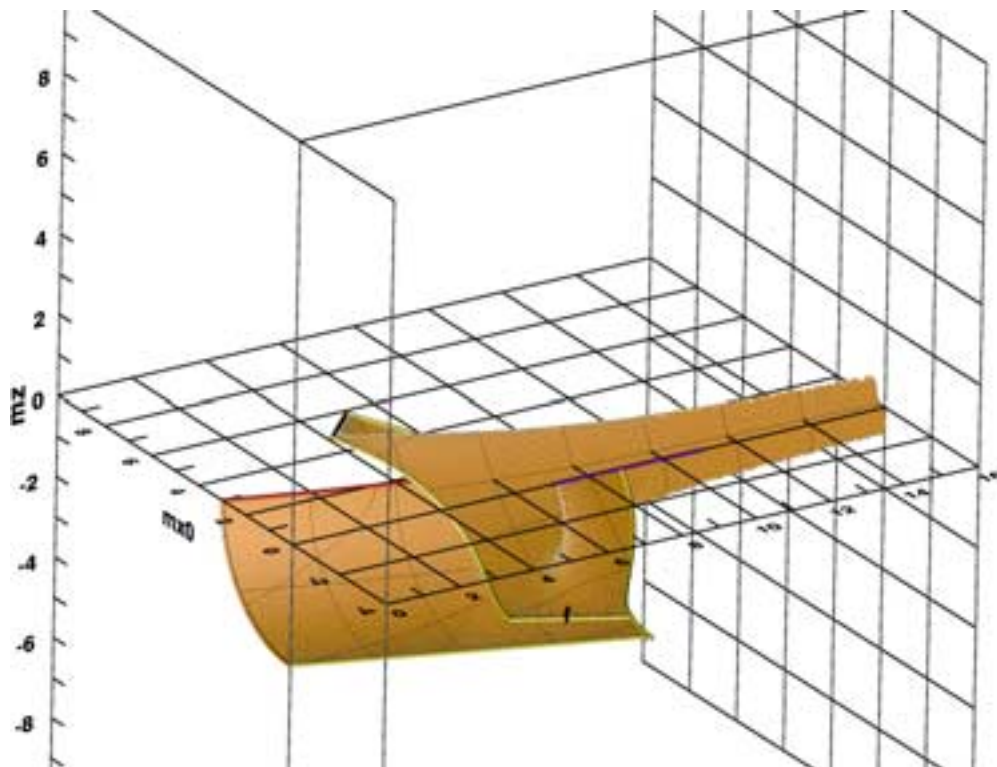Fig. 13. A quarter of layer 3+ in the half space $(m_z, m_{x0}, f \geq 0)$.

Fig. 14.   A quarter of layer 4− in the half space $(m_z, m_{x0}, f \geq 0)$.

Fig. 15.   A quarter of layer 4+ in the half space $(m_z, m_{x0}, f \geq 0)$.
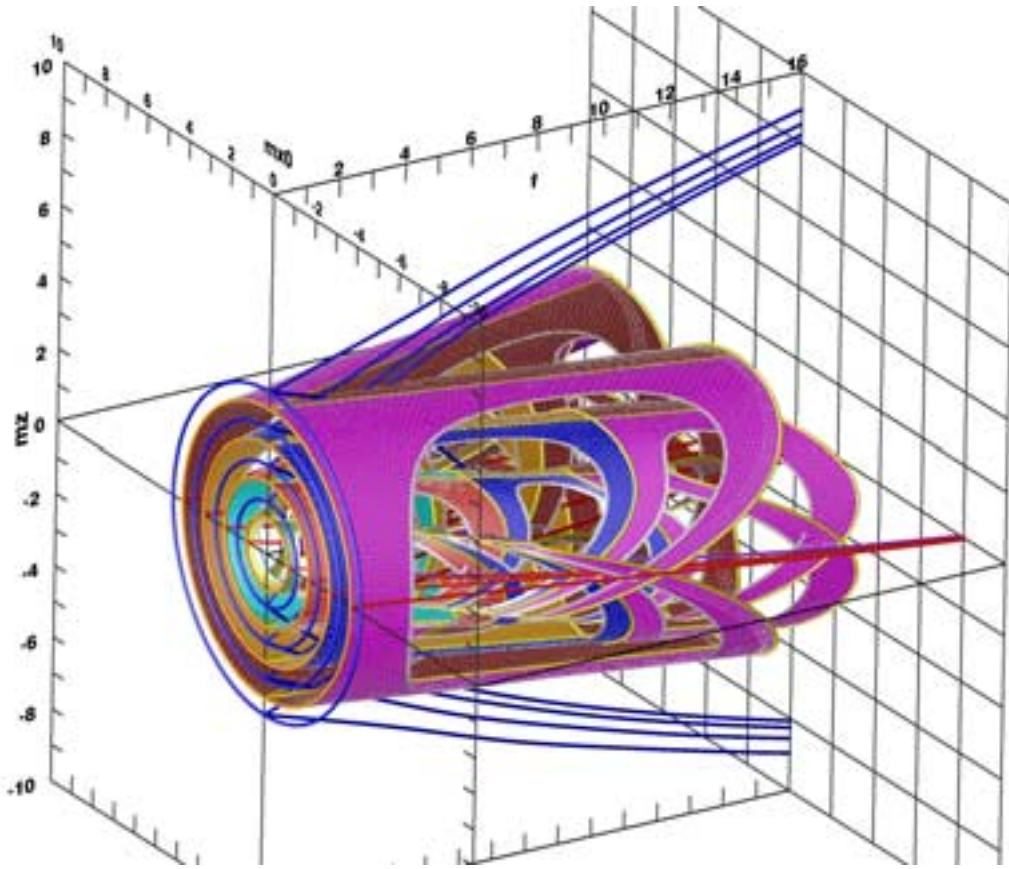
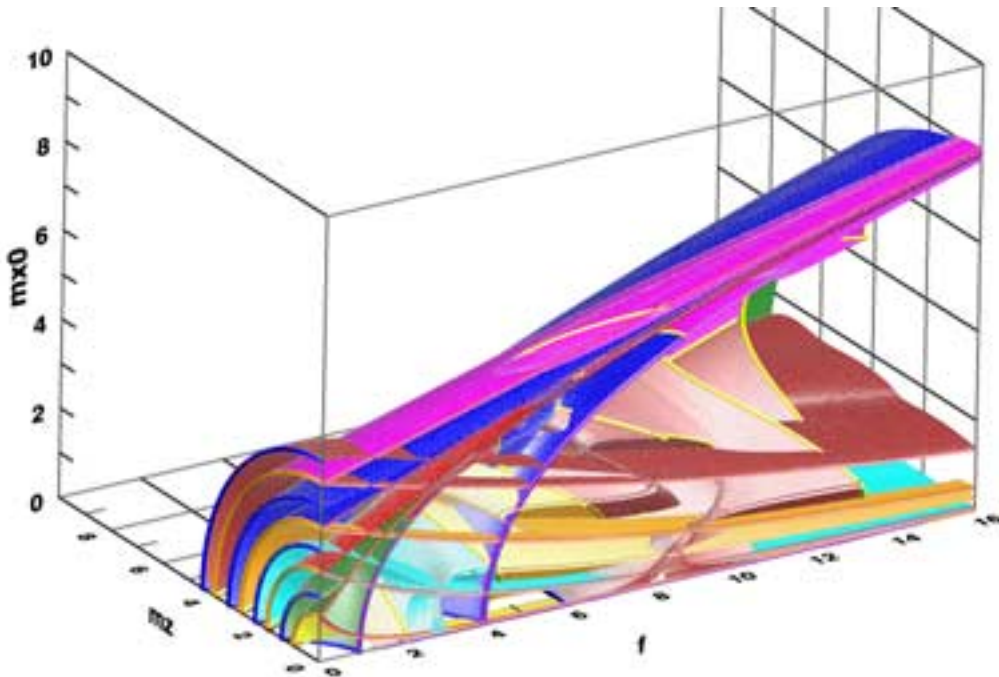Fig. 16. Layers 1±, 2±, 3± and 4± for d around 1 in the entire half space $(m_z, m_{x0}, f \geq 0)$.

Fig. 17. Layers 1±, 2±, 3± and 4± in one octant of the space (m_z, m_{x0}, f).
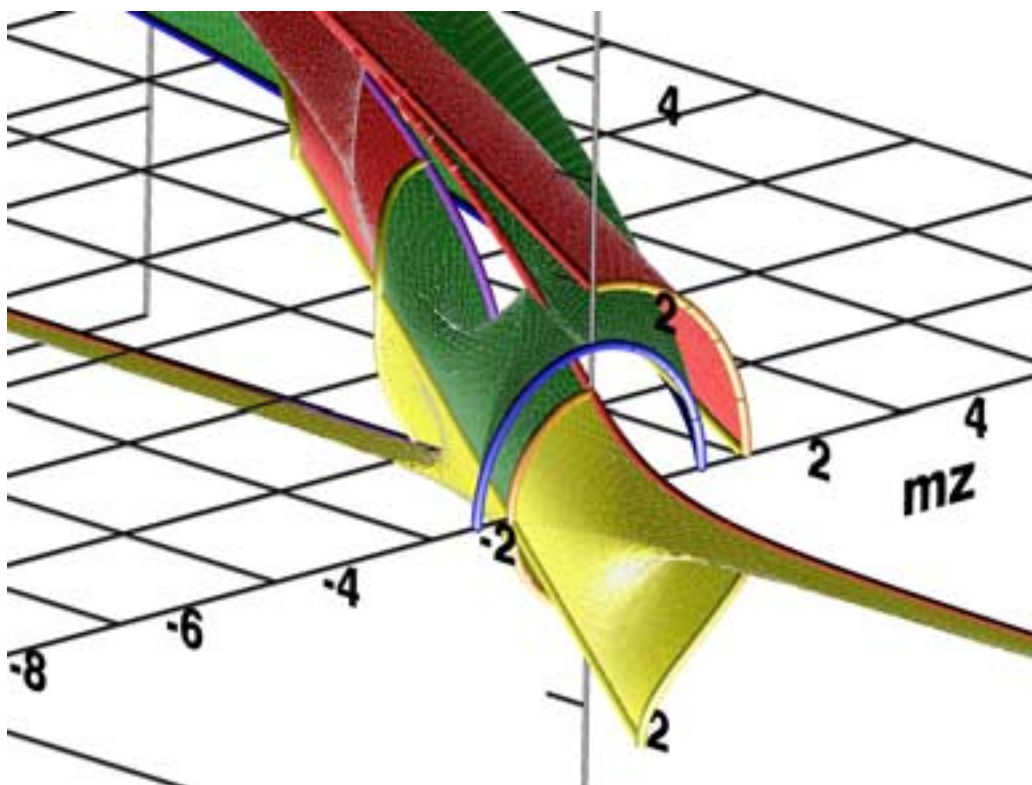
Fig. 18.   The boundary of the quarter of 1− and the quarter of 1+ is the $(N = 1, M = 1)$ path of the buckled rings solution set. The boundary of the quarter of 1− and the two quaters of 2+ is the $(N = 1, M \in]0; 1])$ path of the planar twisted rings solution set and the $(N = 1, M = 0)$ path of the planar untwisted rings solution set.

that are split by the inflectional and noninflectional planar elastica paths belonging to it. In the case of a n^- layer, we further need the buckling curve to part the quarters. For example, to compute one of the four quarters of layer 2-, we take a seed point and we prevent the continuation to either cross any $d = 1$ path or the second buckling curve or the $p = 2$ inflexional planar elastica curve or the $p = 2$ noninflexional elastica curve.

In Figs. 8–15 a quarter of each layer from $n = 1-$ to $n = 4+$ is shown. Having one quarter of a layer, one can get the other three quarters (and hence the entire layer) by using symmetries (13) and (14). So by reflecting each of the quarters, we produced Fig. 16, but we only kept end-shortening values near 1 (i.e $|d − 1|/d$ less than few %). This unravels the connectivity of the layers. In Fig. 17 all the d values are kept but we only show the layers in one octant. Figure 18 shows how the buckled rings $(N = 1, M = 1)$ path is the border that parts layers 1− and 1+, and how the planar ring paths $(N = 1, M \in [0; 1])$ forms the border that parts layers 1− and 2+.

5. Conclusion

In this paper we have shown how a recently introduced continuation algorithm could be used to compute the solution manifold of a boundary value problem arising from elasticity theory. The set of all possible buckled configurations of a twisted rod held in a (aligned) strong anchoring way has been computed. Making use of the symmetries of the problem (both of the material and of the boundary conditions), a reduction of the Kirchhoff equilibrium equations has been performed and the properties of the solution manifold described. Moreover, we have shown how this solution manifold could be split into layers making its display easier, the borders of the layers being the well-known 1D solution set of buckled rings.

Acknowledgments

References

Allgower, E. L. & Georg, K. [1997] "Numerical path following," *Handbook of Numerical Analysis*, Vol. 5, eds. Ciarlet, P. G. & Lions, J. L. (North-Holland), pp. 3–207.

Beyn, W.-J., Champneys, A., Doedel, E., Govaerts, W., Kuznetsov, Y. A. & Sandstede, B. [2002] "Numerical continuation, and computation of normal forms," *Handbook of Dynamical Systems*, Vol. 2, ed. Fielder, B. (Elsevier Science), Chap. 4, pp. 149–219.

Coleman, B. D. & Swigon, D. [2000] "Theory of supercoiled elastic rings with self-contact and its application to DNA plasmids," *J. Elast.* **60**, 173–221.

Dichmann, D. J., Li, Y. & Maddocks, J. H. [1996] "Hamiltonian formulations and symmetries in rod mechanics," *Mathematical Approaches to Biomolecular Structure and Dynamics*, eds. Mesirov, J. P., Schulten, K. & Sumners, D. W., IMA Volumes in Mathematics and Its Applications, Vol. 82, pp. 71–113.

Domokos, G. & Holmes, P. [1993] "Euler's problem, Euler's method, and the standard map; or, the discrete charm of buckling," *J. Nonlin. Sci.* **3**, 109–151.

Domokos, G. & Healey, T. [2001] "Hidden symmetry of global solutions in twisted elastic rings," *J. Nonlin. Sci.* **11**, 47–67.

Gáspár, Z., Domokos, G. & Szeberényi, I. [1997] "A parallel algorithm for the global computation of elastic bar structures," *Comput. Assist. Mech. Engin. Sci.* **4**, 55–68.

Govaerts, W. J. F. [2000] *Numerical Methods for Bifurcations of Dynamical Equilibria* (SIAM, Philadelphia).

Henderson, M. E. [2002] "Multiple parameter continuation: Computing implicitly defined k-manifolds," *Int. J. Bifurcation and Chaos* **12**, 451–476.

Hoffman, K. A., Manning, R. S. & Paffenroth, R. C. [2002] "Calculation of the stability index in parameter-dependent calculus of variations problems: Buckling of a twisted elastic strut," *SIAM J. Appl. Dyn. Syst.* **1**, 115.

Karolyi, G. & Domokos, G. [1999] "Symbolic dynamics of infinite depth: Finding global invariants for BVPs," *Physica* **D134**, 316–336.

Keller, H. B. [1976] *Numerical Solution of Two Points Boundary Value Problems* (SIAM, Philadelphia).

Li, Y. & Maddocks, J. H. [1994] "On the computation of equilibria of elastic rods, part I: Integrals, symmetry and a hamiltonian formulation," *J. Comput. Phys.*, preprint.

Love, A. E. H. [1944] *A Treatise on the Mathematical Theory of Elasticity*, 4th edition (Dover Publishing, NY).

Neukirch, S. & Henderson, M. E. [2002] "Classification of the spatial clamped elastica, part I: Symmetries and zoology of solutions," *J. Elast.* **68**, 95–121.

Paffenroth, R. C. [1998] "VBM and MCCC: Packages for objected oriented visualization and computation of bifurcation manifolds," in *Object Oriented Methods for Interoperable Scientific and Engineering Computing*, eds. Henderson, M. E., Anderson, C. R. & Lyons, S. L. (SIAM), pp. 255–263.

van der Heijden, G. H. M. & Thompson, J. M. T. [2000] "Helical and localised buckling in twisted rods: A unified analysis of the symmetric case," *Nonlin. Dyn.* **21**, 71–79.